GEOPHYSICS, VOL. 76, NO. 3 (MAY-JUNE 2011); P. R69–R80, 14 FIGS., 1 TABLE.
10.1190/1.3554652

Multiple-domain, simultaneous joint inversion of geophysical data with application to subsalt imaging

Michele De Stefano[1], Federico Golfré Andreasi[1], Simone Re[1], Massimo Virgilio[1], and Fred F. Snyder[2]

ABSTRACT

We describe an effective method for joining the benefits of inversion of different kinds of measurements. We show the simultaneous joint inversion objective function, which allows users to link different inversion domains, like seismic with gravity or seismic with magnetotellurics. This function can be extended to any number of domains and does not require that they be sampled on the same grid. Our parallel implementation allowed us to scale well with large volumes of data and a large number of unknowns, and it has already been included in production workflows. Furthermore, it is generic and constitutes a framework where new inversion techniques can be easily plugged in. We also present two different ways of linking various inversion domains for establishing relationships between different model domains and how they can be chosen and used to achieve the best result. Applications of the algorithm using synthetic and field data produce model features generally not achievable with single-domain inversions. Specifically, we applied our technique to real data from the Walker Ridge area in the Gulf of Mexico, and we used the results to reinterpret and remigrate seismic data. The final migrated section clearly found improved quality with respect to previous efforts. Our results document the fundamental importance of integrating nonseismic methods with seismic techniques to increase the image quality of geologically complex areas.

INTRODUCTION

The term joint inversion embraces a broad set of techniques, and it is often used to identify any type of algorithm aimed to obtain data integration. In this paper, we will call model domain or simply domain the space into which our inversion results will be placed. We will address as single-domain inversion any of the standard inversion algorithms that invert a single type of data to estimate a single type of unknown. For example, refraction tomography is a single-domain inversion technique because it inverts the arrival times of refracted seismic waves to obtain a velocity model. The velocity is the unknown and also the domain of this inversion technique.

As a further step, we can identify in literature some examples of what we call single-domain joint inversion (SDJI). With this term, we will address all the algorithms that try to invert different data types to obtain a single type of unknown. For example, Yang and Tong (1988) propose the joint inversion of direct-current (DC), transient electromagnetic (TEM), and magnetotelluric (MT) data to estimate the resistivity; Li and Oldenburg (2000) use borehole and surface magnetic data to invert for the susceptibility; Rossi and Vesnaver (1997) take reflected and refracted arrivals and invert for the seismic P-velocity; Fu (2004) uses a neural network to invert for the acoustic impedance, integrating seismic data, well data, and geological information.

We call another type of joint inversion, cooperative joint inversion (CJI). An example can be found in Dell'Aversana (2001), where the author presents a methodology for integrating seismic and electromagnetic data. In that paper there are two model domains: seismic, represented by seismic velocity, and electromagnetic, represented by resistivity. This type of joint inversion is called cooperative because first we invert in one model domain (for example, the seismic domain); then, we convert the final model into the other domain with some empirical law. At this point, we invert for the other domain, we convert the result back into the first domain, and then reiterate the procedure until a specific quality control stops the process. We can

Manuscript received by the Editor 27 April 2010; revised manuscript received 8 November 2010; published online 5 May 2011.
[1]WesternGeco, Milan, Italy. E-mail: mstefano@slb.com; fandreasi@slb.com; sre@slb.com; mvirgilio@slb.com.
[2]WesternGeco, Houston, Texas, U.S.A. E-mail: fsnyder@slb.com.

find an alternative approach to CJI in Hu et al. (2009), where one model domain acts as a constraint for inversion of the other, and the roles of the two domains are iteratively switched.

We call a more evolved joint inversion technique *simultaneous joint inversion* (SJI). In SJI, we have different data types (for example, seismic refraction arrival times and gravity measurements), and we try to simultaneously invert them with a link between the model domains. An early example of this technique can be found in Haber and Oldenburg (1997); the authors proposed to link two different model domains minimizing the difference between structural operators computed on the Laplacian of each of the model functions. Another example of the utilization of a structural link can be found in Gallardo and Meju (2004) where the solution to a bidimensional, linear, seismic-electromagnetic SJI problem is achieved using the cross-gradients link as a constraint in a constrained optimization algorithm. De Stefano and Colombo (2007) proposed a different approach; links are not used as constraints, but they are inverted together with the domains' objective functions. With this approach, we can link the model domains also with an empirical law that is not strictly exact for the region of interest; the link influences the objective function not as a rigid constraint, like in Gallardo and Meju (2004), but in a statistical or least-squares sense. A similar use of empirical link equations can also be found in Jegen et al. (2009).

We will present further improvements to the previously discussed SJI algorithms. We formulate the problem in a way that takes into account the integration of three-dimensionality of the subsurface, its nonlinearity, its independent sampling, and potentially different norms. We show that this new formulation can be extended to any number and type of domains and links. We also demonstrate the different weights of geometrical and empirical link equations and suggest how to use them.

After an initial mathematical formulation, we show applications to synthetic and real, 3D data sets. We prove that our technique can lead to final models where the benefits of every single-domain inversion are obtained, resulting in a better subsurface estimate.

METHOD

In Table 1, we provide a reference to the most important mathematical symbols used in this paper. Furthermore, some symbols may have a footer index (e.g., i or j) to specify the particular domain or link to which the symbol is related.

Other important mathematical symbols are:

- α_i, for the weight of the ith domain.
- β_j, for the weight of the jth link function Ψ_j.
- p_i, for the misfit norm.

Compact formulation

The most compact form of the proposed multiple-domain SJI objective function can be expressed in equation 1 as follows:

$$\Phi_{\mathrm{SJI}}(\mathbf{m}) = \sum_i \alpha_i \Phi_i(m_i(\mathbf{r})) + \sum_j \beta_j \int_{U_j \subseteq V_{\mathrm{int}}} \Psi_j(\mathbf{m}) dv, \quad (1)$$

where

$$\Phi_i(m_i(\mathbf{r})) = \left\| \mathbf{W}_{d,i}(\mathbf{g}_i(m_i) - \mathbf{d}_i) \right\|^{p_i} + \int_{V_i} \Gamma_i(m_i - m_{\mathrm{pri},i}) dv, \quad (2)$$

and $\Psi_j(\mathbf{m})$ is a generic cost function that links all the domains involved in the inversion; V_{int} is the intersection of all volumes V_i that are occupied by the single-domain model functions. This expression allows us to summarize all possible forms it can take in our implementation and examples. Notice that $\mathbf{r}$ is a continuous position vector and that the continuous m_i functions depend on it. As briefly explained in Table 1, we will often drop the dependency on $\mathbf{r}$ from model functions to simplify the readability of mathematical expressions. It is intended anyway that, for example, m_i is the same as $m_i(\mathbf{r})$. The reader is referred to Table 1 for the terms that depend on $\mathbf{r}$.

If we assume that modeling and data errors are both Gaussian, equation 1 is the Bayesian objective function of SJI (Mosegaard and Tarantola, 1995; Ulrych et al., 2001; Malinverno and Briggs, 2004; Tarantola, 2005). In fact, taking $p_i = 2$, if we reorder equation 1 such that in equation 3 we group the sum of all the data misfits into one term (joint likelihood) and into another term all the regularizations plus the sum of link terms

$$\Phi_{\mathrm{SJI}}(\mathbf{m}) = \left(\sum_i \alpha_i \left\| \mathbf{W}_{d,i}(\mathbf{g}_i(m_i) - \mathbf{d}_i) \right\|^2 \right) + \eta \int_{V_i} \left(\sum_i \frac{\alpha_i}{\eta} \Gamma_i(m_i - m_{\mathrm{pri},i}) + \sum_j \frac{\beta_j}{\eta} \delta_{U_j \subseteq V_{\mathrm{int}}}(\mathbf{m}) \Psi_j(\mathbf{m}) \right) dv \quad (3)$$

with

$$\delta_{U_j \subseteq V_{\mathrm{int}}}(\mathbf{m}) = \begin{cases} 1 & \mathbf{m} \in U_j \\ 0 & \text{otherwise} \end{cases} \quad (4)$$

we can see similarities with the classical Bayesian objective function. In fact, equation 3 can be rewritten as

Table 1. Table of the most important symbols used in mathematical formulation.

Table of Symbols	
$\mathbf{r}$	Position vector
m or $m(\mathbf{r})$	Model function (continuous)
$\mathbf{m}$ or $\mathbf{m}(\mathbf{r})$	Vector of all model functions
m_{pri} or $m_{\mathrm{pri}}(\mathbf{r})$	A-priori model function (continuous)
$\mathbf{d}$	Observed data vector
$\mathbf{g}$	Vectorial forward function
$\mathbf{W}_d$	Matrix of data weights
$\Gamma(m - m_{\mathrm{pri}})$	Regularization function
λ	Regularization weight
V	Volume of interest, occupied by the model function
U	A subvolume of V, where links have to be evaluated
$\Phi(m)$	Single-domain cost function
$\Psi(\mathbf{m})$	Link function
$\Phi_{\mathrm{SJI}}(\mathbf{m})$	The SJI cost function
$*$	Convolution product

$$\Phi_{\mathrm{SJI}}(\mathbf{m},\eta) = \|\mathbf{W}_d(\mathbf{d}-\mathbf{g}(\mathbf{m}))\|^2 + \eta\|R(\mathbf{m})\|^2 \quad (5)$$

where

$$R(\mathbf{m}) = \left(\sum_i \frac{\alpha_i}{\eta}\Gamma_i(m_i - m_{\mathrm{pri},i}) + \sum_j \frac{\beta_j}{\eta}\delta_{U_j\subseteq V_{\mathrm{int}}}(\mathbf{m})\Psi_j(\mathbf{m})\right)^{1/2} \quad (6)$$

and $\mathbf{W}_d$ is a block diagonal matrix whose diagonal elements are $\mathbf{W}_{d,i}$ matrices. The nonlinear covariance term $\|R(\mathbf{m})\|^2$ clearly sums the contributions of single-domain regularizers and of the links. The extension to $p_i \neq 2$ can be obtained assuming, for data misfits, the generalized Gaussian probability density instead of the ordinary Gaussian distribution (this is left as an exercise for the reader). We stress that equation 1 neither sets any limit for the number of domains or links, nor requires sampling of different domains on the same grid.

In our implementation, we use two kinds of links: empirical and structural.

Empirical links

Empirical links relate two or more domains through a law. For example, Gardner's law

$$\varrho = a \cdot v_P^b \quad (7)$$

establishes an empirical link between the seismic P-velocity and the rock density. It is translated into the cost function

$$\Psi(m_1,m_2) = \left|a \cdot m_1^b - m_2\right|^2 \qquad m_1 = v_P,\ m_2 = \varrho. \quad (8)$$

Another example is the log-linear law, which we often used to link resistivity to P-velocity in a seismic-MT SJI:

$$\ln\rho = a \cdot v_P + b \quad (9)$$

and its corresponding cost function,

$$\Psi(m_1,m_2) = |a\cdot m_1 - \ln m_2 + b|^2 \qquad m_1 = v_P, m_2 = \rho. \quad (10)$$

Structural links

Structural links relate domains through geometrical properties only. We implemented the cross-gradients cost function in equation 11

$$\Psi(m_1,m_2) = |\nabla m_1 \times \nabla m_2|^2. \quad (11)$$

This function requires the parallelism between model gradients. It is well known that gradients are perpendicular to the edges of the objects (Pratt, 1991). As a consequence, this forces the output models to have the same shapes in the same spatial positions.

Implementation details

Figure 1 represents our actual software implementation of equation 1. There is an SJI core block, which runs the solver and which is able to assemble the joint objective function starting from single domain and link contributions. Then, there is a domain manager block for each domain that is involved into the joint inversion run. The user decides how many domains to simultaneously invert, how many links to use, and how the U_j regions of links are shaped. When the user chooses only one domain and no link, we have a single-domain inversion. With this structure, adding a new domain requires developing only a new domain manager, without touching the SJI core at all. Furthermore, we have decoupled the SJI algorithm from single-domain algorithms. In this way, each model domain is entirely managed by the corresponding domain manager, and the SJI core block does not require any further information on the specific objective function of each single-domain. The SJI core block communicates with each domain or link manager to retrieve the corresponding value and gradient of each single-domain or link objective function. SJI core collects those values into the SJI objective function during the iterations of the solver. The infrastructure of Figure 1 is particularly suited to be implemented in an object-oriented programming language.

Our SJI implementation is a nonlinear minimization of an L_2 norm cost function that means that, in equations 1 and 2, we used $p = 2$. An exception to this rule is the cost function for reflection tomography, where p can be chosen to be either 2 or 1.5. The choice to use $p = 1.5$ is taken empirically by the user, when the inversion with $p = 2$ fails to give any good result. This option is a legacy from the existing, single-domain, reflection tomography algorithm. We use a nonlinear conjugate gradients solver (NLCG) (Teukolsky et al., 2007) because of its efficient memory usage. For the underlying linear algebra we use the Portable Extensible Toolkit for Scientific Computation (PETSc) (Balay et al., 1997, 2008, 2009). In this way, with large data sets, our software can scale well on a large number of nodes in a parallel environment. For regularization, we have options to use differential operators, such as Laplacian or gradients (Berdichevsky and Dmitriev, 2002), or a preconditioner, or both.

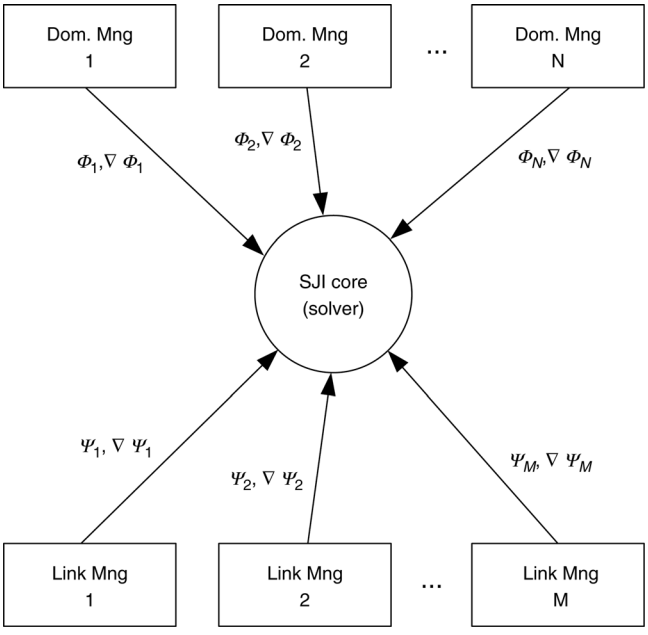

Figure 1. Logical software implementation of SJI. There is one domain manager for each model domain and one link manager for each link. The SJI core block communicates with each domain or link manager to retrieve the corresponding value and gradient of each single domain or link objective function. SJI core collects those values into the SJI objective function during the iterations of the solver.

To overcome the difficulties arising when applying the same link for the whole models, the implementation of link terms allows the user to define space variant links. By properly masking the models, we can associate a specific link to a specific spatial region. As shown mathematically in equation 1, the integration volume for each link condition is U_j, which is a subset of the intersection volume V_{int} and can be different for each link. A possible configuration of integration volumes for links is shown in Figure 2, where the three regions for three links are disjoint. Nothing prevents us also using partially overlapping regions or using three links that cover all the V_{int} region at the same time. We could also conceive a situation where the three model domains do not have an intersection region common to all three of them at the same time. It is possible to have intersection regions common only to two domains at the same time. In this case, we can use as many link functions as the number of intersection regions with this criterion: for each intersection region we use a link that involves only the model domains that have a non-null intersection with the region itself.

Furthermore, because equation 1 is written in continuous spatial coordinates (see Table 1 again; $\mathbf{r}$ is a continuous spatial position vector), we do not require that each model domain is sampled with the same grid or mesh. We only require that each link term is evaluated on the proper U_j spatial region.

We have no particular algorithm to automatically compute the weights present in equations 1 and 2, but we have an empirical way to work with those expressions. The user first estimates single-domain weights, performing trial and error with single-domain inversions. After determining the single-domain weights, the SJI weights (α_i and β_j) are estimated in a similar manner. To avoid the user treating completely unrelated SJI weights, we preemptively normalize Φ_i functions to 1, before applying α_i weights. The correct way to balance single-domain objective functions should be to bring them to have the same minimum value. We cannot do this simply because we do not know which is the minimum of those functions (otherwise, we did not need an inversion at all). Thus, determining α_i, relative power to each domain after a preemptive normalization is automatically assigned. Prenormalization of Ψ_j functions is performed in the same way, even if we know that they all have a theoretical zero minimum value. This is necessary to bring them to the same initial numerical power as Φ_i functions. User-defined β_j weights are applied after this prenormalization.

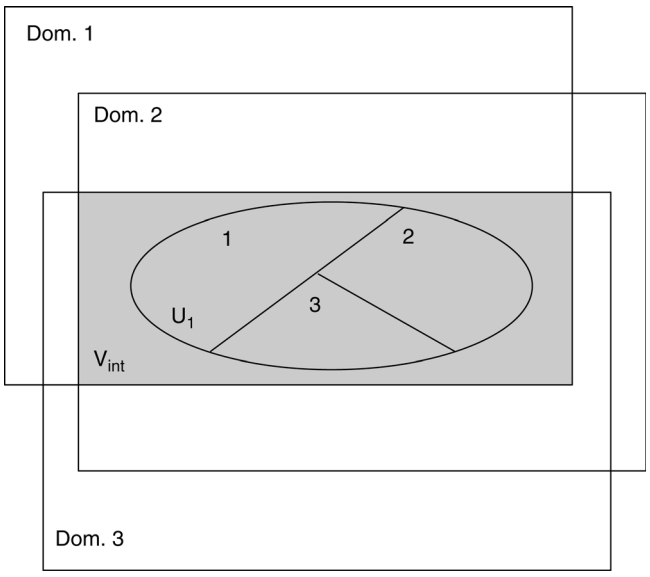

Figure 2. Logic for the definition of a space variant link. If we have three different model domains, SJI links can work potentially on the whole intersection region V_{int} (the region in gray). Here we decided to use three different links, each of them working only in a subset of V_{int}. We create a mask that marks with 1 the region U_1, with 2 the region U_2 and with 3 the region U_3. For simplicity, we have drawn nonoverlapping regions, but nothing prevents using partially overlapping ones.

In the following discussion, we give some examples of single-domain objective functions that we plugged into equation 1 in place of Φ_i. We want to stress that we developed the algorithm only for joining different inversions, but we did not make any research on the single-domain algorithm themselves. We integrated in SJI existing single-domain algorithms and programed a corresponding domain manager for each of them, without being concerned with the reasons behind the choices for a particular single-domain objective function.[3] Explaining details on a specific single-domain objective function is outside the scope of this paper. In equation 2, $\mathbf{g}_i(m_i)$ can potentially have any mathematical form, and its evaluation is performed by the specific domain manager of each domain involved in SJI, using exactly the same computations performed by the corresponding single-domain technique. The SJI core block of Figure 1 serves as a common inversion framework for any single-domain technique that can provide the evaluation of an objective function (and of its gradient).

Gravity and full tensor gradiometry joint objective function

For gravity and full tensor gradiometry (FTG), the domain objective function in equation 2 was modified as follows:

$$\Phi(m(\mathbf{r})) = \left|\mathbf{W}_{d,1}(\mathbf{g}_1(m) - \mathbf{d}_1)\right|^2 + \eta \cdot \left|\mathbf{W}_{d,2}(\mathbf{g}_2(m) - \mathbf{d}_2)\right|^2 + \int_V \Gamma\left(m - m_{\text{pri}}\right) dv \tag{12}$$

where $\mathbf{g}_1$ is the standard gravity-forward operator, and $\mathbf{g}_2$ is the FTG forward operator (or vice versa). The relative weight between standard gravity and FTG is represented by η.

For forward modeling and regularization, we adopted the approach described in Li and Oldenburg (1996, 1998), for the regularization function:

$$\Gamma\left(m - m_{\text{pri}}\right) = \alpha_s\left\{w(\mathbf{r})\left[m - m_{\text{pri}}\right]\right\}^2 + \alpha_x\left\{\frac{\partial w(\mathbf{r})\left[m - m_{\text{pri}}\right]}{\partial x}\right\}^2 + \alpha_y\left\{\frac{\partial w(\mathbf{r})\left[m - m_{\text{pri}}\right]}{\partial y}\right\}^2 + \alpha_z\left\{\frac{\partial w(\mathbf{r})\left[m - m_{\text{pri}}\right]}{\partial z}\right\}^2 \tag{13}$$

[3]Our work consisted only in developing the most general integration technique for possibly any single-domain inversion and not to develop single-domain inversions, too. In any case, SJI cannot properly work if single-domain algorithms are not robust and effective on their own.

where α_s, α_x, α_y and α_z are coefficients that affect the relative importance of different components in the regularization function, and $w(\mathbf{r})$ is a weighting function dependent on forward sensitivity that contrasts the decay of the gravity field. Refer to Li and Oldenburg (2000) for a similar formulation

$$w(\mathbf{r}) = \left\| \begin{bmatrix} \frac{d\mathbf{g}_1}{dm(\mathbf{r})} \\ \sqrt{\eta}\frac{d\mathbf{g}_2}{dm(\mathbf{r})} \end{bmatrix} \right\|_2 \quad (14)$$

as seen in equation 14. Note that, taken alone, equation 12 allows us to perform a single-domain joint inversion of gravity and FTG data. Suppressing one of the two forward terms allows us to perform either a gravity or an FTG single-domain inversion.

First breaks objective function

For first breaks (FB) inversion, the domain objective function in equation 2 was modified as

$$\Phi(m(\mathbf{r})) = |\mathbf{W}_d(\mathbf{g}(m) - \mathbf{d})|^2 + \lambda \int_V \left|\nabla^2 (m - m_{\text{pri}})\right|^2 dv. \quad (15)$$

Common-image-point tomography

For common-image-point (CIP) tomography, we integrated into SJI an existing technology based on Woodward et al. (1998) and Osypov et al. (2008) where the objective function uses a preconditioner and a unit regularizer. Equation 2 of the domain objective function becomes

$$\Phi(m(x)) = |\mathbf{W}_d(\mathbf{g}(h * x) - \mathbf{d})|^p + \lambda \int_V |x - x_0|^2 dv, \quad (16)$$

where

$$m = h * x$$

$$m_0 = h * x_0$$

and p can be empirically chosen to be either 2 or 1.5. Minimization of this function is performed into the transformed domain x, which is related to m through a convolution with a low-pass filter h; m_0 and x_0 are the starting models into the direct and transformed domain, respectively. Due to difference in existing FB and CIP modeling applications and our inability to combine them, we end up having two different model domains for seismic velocity. Further, due to anisotropy, keeping distinct domains for CIP and FB inversions is justified. In general, CIP tomography is more sensitive to quasivertical propagation and FB tomography is more sensitive to quasihorizontal propagation. With our implementation, we allow the user to perform a reflection-refraction SJI with different spatial resolutions in the two model domains. In case anisotropy is ignored, CIP and FB modeling can be done with same sampling and be joined using a trivial identity link.

Magnetotelluric objective function

The objective function for MT inversion is the same as that presented in Mackie et al. (2001) and seen in equation 17

$$\Phi(m(\mathbf{r})) = |\mathbf{W}_d(\mathbf{g}(m) - \mathbf{d})|^2 + \lambda \int_V \left|\nabla^2 (m - m_{\text{pri}})\right|^2 dv. \quad (17)$$

Its mathematical form is identical to that used for FB in equation 15, but our single-domain implementation is nonlinear (for details of the method, see Mackie et al., 1993; Mackie and Madden, 1993; and Zhang et al., 1995).

EXAMPLES

Synthetic example

The results we present come from simulations on density and velocity synthetic models that are very similar to the dipping dykes example presented by Li and Oldenburg (1998). The synthetic velocity model consists of two dikes dipping in opposite directions and having different widths and lengths, but the same x strike direction. Figure 3 shows this model in one cross section and in one plan section. The velocities of the two dykes are 5000 m/s and 6000 m/s respectively. The background velocity is 2000 m/s.

The corresponding density synthetic model is obtained applying the Gardner's law in equation 7, with $b = 0.25$ and $a = 309.5984\ \text{kg/m}^3 \cdot (\text{s/m})^{0.25}$. The densities of the two dykes are $2603.40\ \text{kg/m}^3$ and $2724.81\ \text{kg/m}^3$, respectively; the background density is $2070\ \text{kg/m}^3$.

For the seismic domain, we simulate first-arrival times from 16 sources and 64 receivers. Sources are evenly distributed on the surface with a spacing of about 3160 m in x and y; receivers have an equal spacing of about 1200 m in x and y. All channels are always active while shooting, for a total of 1024 first-arrival times. We add a zero-mean, random, white Gaussian noise with a 10 ms standard deviation to each data sample. The two model domains have the same sampling, with 20 cells along x, 20 along y, and 10 along z.

For the gravity domain, we simulate the vertical component of the gravity field, measured on the surface at 441 evenly spaced stations. The spacing between stations is 500 m in both directions. We add a zero-mean, random, white Gaussian noise with a 10 μGal standard deviation to each data sample.

The initial model for the seismic domain model is a vertical velocity gradient with a starting velocity of 2500 m/s and a final velocity of 5500 m/s. The initial density domain model is a volume with a uniform density of $2070\ \text{kg/m}^3$.

Figure 4 shows the output of the two inversions carried out separately on the velocity and density domains. Figure 5 shows the results obtained from a joint inversion that uses Gardner's law as a link. We used equation 1 with $i = 1,2$ and $j = 1$ substituting the objective function of first breaks (equation 15) for Φ_1, the gravity objective function (equation 12, with $\eta = 0$) for Φ_2, and the Gardner's objective function (equation 8) for Ψ_1. For the weights, we used $\alpha_i = 1$ and $\beta_1 = 1$. The parameters of Gardner's law used for the inversion are the same as those used to build the synthetic density model. Results from SJI (Figure 5) are more focused than those of single-domain inversions. Furthermore, Figure 6 shows that the outputs of SJI follow more closely Gardner's law suggesting the effectiveness of empirical link. The points of the scatterplot (Figure 6b) are all below the theoretical curve because gravity inversions always output

spread densities, which rarely reach the true density value (Li and Oldenburg, 1998). Similarly, Figure 7 shows the results obtained by an SJI with a cross-gradients link. Computing equation 11 and integrating it, we obtain 985.55 $kg^2/(s \cdot m^4)^2$ for the single-domain results and 545.41 $kg^2/(s \cdot m^4)^2$ for those coming from SJI. Figures 8 and 9 allow us to evaluate the effectiveness of the link. Furthermore, Figure 9 verifies the parallelism of the gradients because we can detect a direct proportionality between the main gradient directions of velocity and gravity models.

The synthetic example shows that empirical law is better than cross-gradients. We also tried to make an SJI with both the Gardner's law and cross-gradients, but the result is not so different from the one obtained only with the empirical law. Returning again to Figure 9, we note, as expected, that gradients close to zero are nearly uncorrelated. This means that cross-gradients impose a strong link only in the regions where some discontinuities are present (typically, the structure borders). On the other hand, an empirical law establishes a strong link everywhere. Another point in favor of the empirical link is that, for 3D inversions, the computational cost of an empirical law is about one-third that of the cost of the cross-gradients. This is because the latter has to compute the three gradient components, whereas the former has to evaluate only a point-to-point relation.

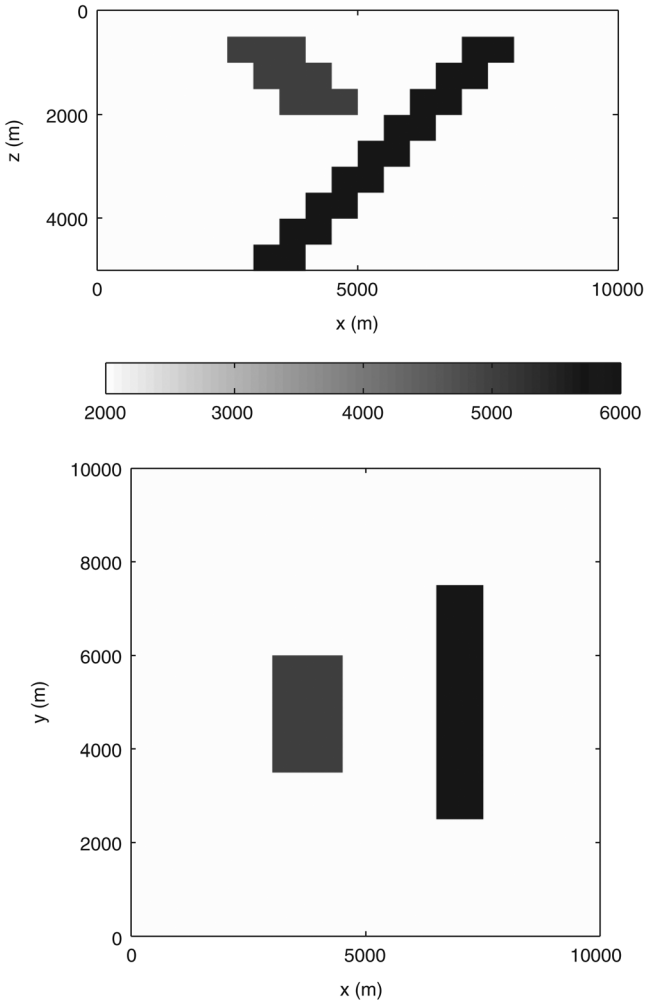

Figure 3. Cross section (at y = 5000 m) and plan section (at z = 1250 m) of the velocity synthetic model. The velocities of the two dykes are 5000 m/s and 6000 m/s respectively. The background velocity is 2000 m/s. The synthetic density model is obtained from this one through a Gardner's law with b = 0.25 and $a = 309.5984\ kg/m^3 \cdot (s/m)^{0.25}$. The values of the two dykes in the density domain are $2603.40\ kg/m^3$ and $2724.81\ kg/m^3$, respectively.

Real data example

Because of formation of the Jurassic Louann salt during continental crust prebreak-up and subsequent early salt movement due to gravity spreading toward the cooling and sinking oceanic plate, the Gulf of Mexico is a tectonically favorable exploration province, albeit very complex in places (Campbell et al., 2009).

A robust approach involving seismic and nonseismic measurements is very important in the Green Canyon-Garden Banks-Keathley Canyon-Walker Ridge areas because the salt complexity is extremely challenging, even with the latest acquisition methods (Campbell et al., 2009). However, using geologic information and multidomain integration to augment normal seismic data is proving successful (Campbell et al., 2009). These methods help better facilitate interpretation of the entire salt body, which is important not only for a better salt model and reservoir image, but also to better understand possible reservoir compartmentalization

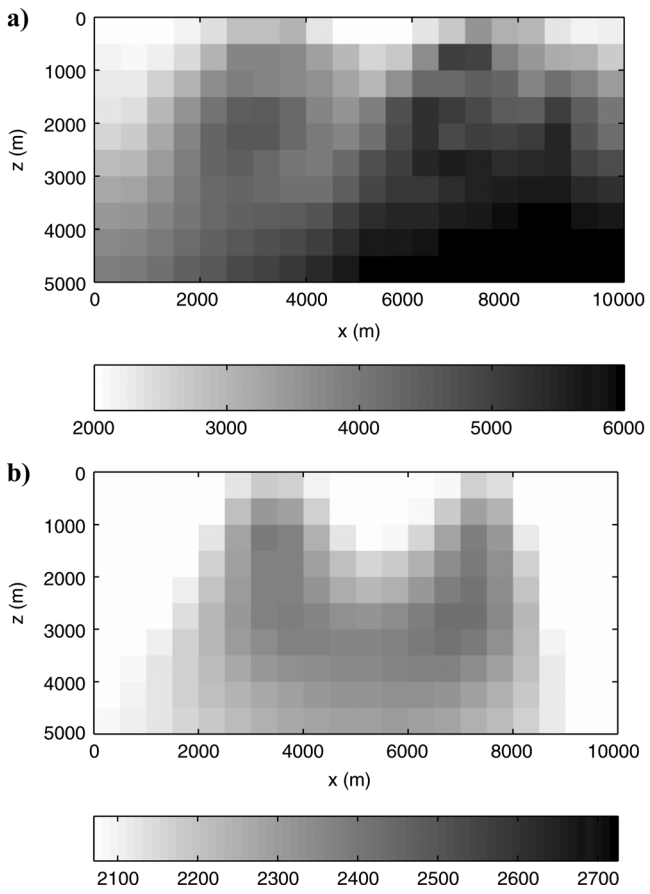

Figure 4. Results of single-domain inversions (cross section at y = 5000 m): (a) FB inversion; (b) gravity inversion. The gravity color scale spans the interval $[2070, 2725]\ kg/m^3$, which is the same range as the density synthetic model.

mechanisms, abnormal pressure cells, and other exploration risks (Andersen and Bodger, 2005).

In this example, we took an existing multiclient seismic structural framework, removed a portion of the salt, and ran several iterations of SJI with CIP tomography and marine MT, obtaining the final SJI velocity model. We know from previous work that the salt must have the shape it has in the structural framework, and we want our SJI to reconstruct that shape. It is like making a synthetic test with real data. The starting model is shown in Figure 10, where the portion of the salt that we removed is bounded between dashed and solid lines. To perform the SJI, we used equation 1 with $i = 1,2$ and $j = 1$, substituting the objective function of CIP tomography (equation 16) for Φ_1, the MT objective function for Φ_2, and the log-linear objective function (equation 9) for Ψ_1. Analysis of well logs drove us to parameterize the log-linear law with $a = 0.0025$ s/m and $b = -9.1206$. For the weights of the seismic and resistivity domains we used $\alpha_1 = 1$, $\alpha_2 = 5$, and $\beta_1 = 5$.

Figure 11 shows a comparison between the final velocity coming from single-domain inversions and the velocity from SJI. On the seismic side, we inverted only a small portion of the whole model; this region was the one directly beneath the salt hole.

The initial model used for the MT domain was very similar to the velocity model of Figure 10, but we did not remove any salt. It

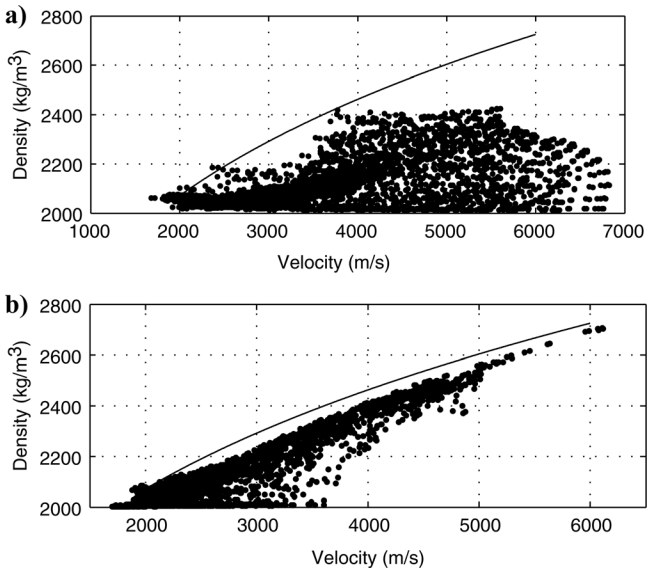

Figure 6. Crossplot velocity/density of the output models of: (a) single-domain inversion, and (b) joint inversion with a Gardner's law link of the synthetic data. The continuous line is the theoretical Gardner's law.

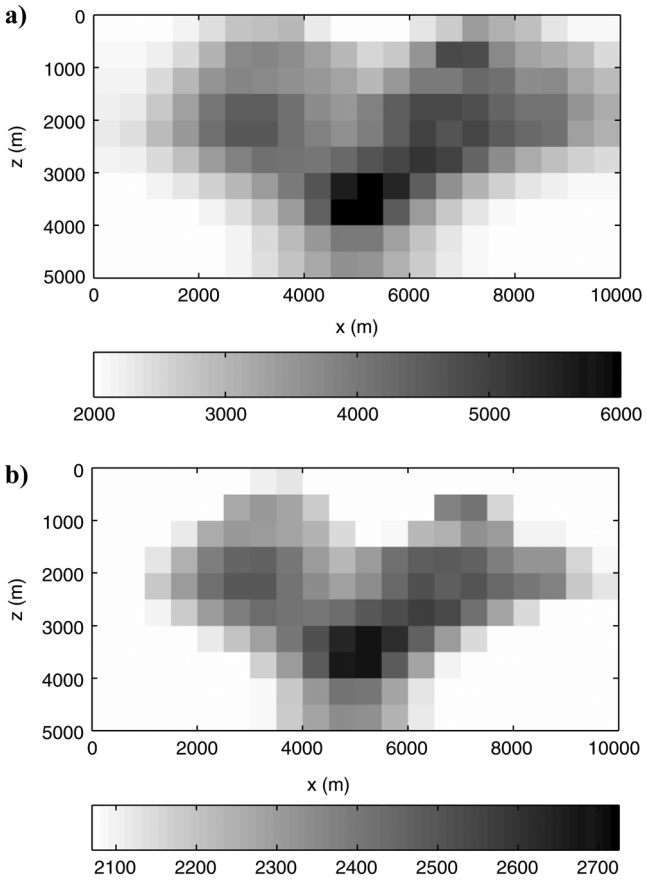

Figure 5. Results of a joint inversion with the Gardner's law (cross section at y = 5000 m): (a) velocity;(b) density. The gravity color scale spans the interval $[2070, 2725]$ kg/m^3, which is the same range as the density synthetic model.

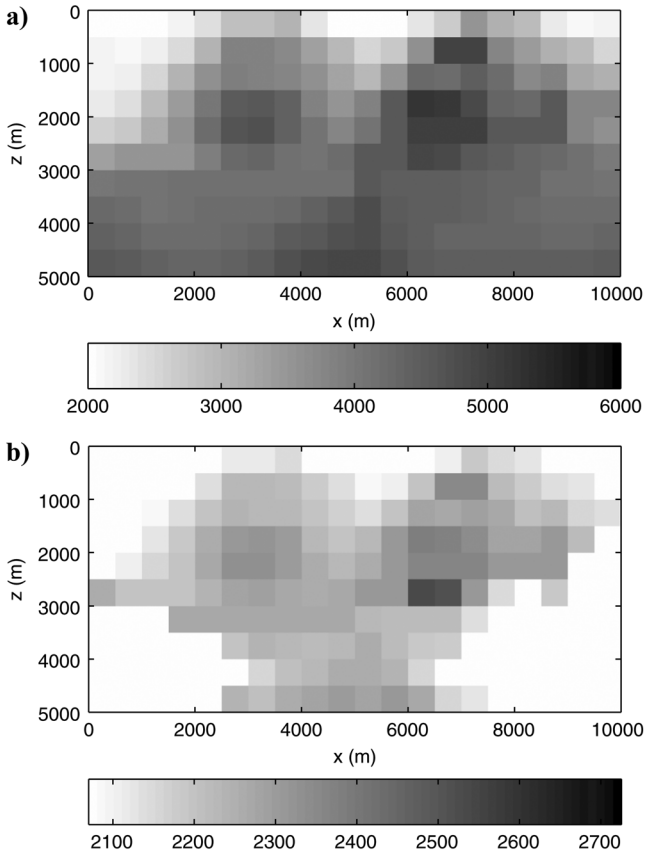

Figure 7. Results of a joint inversion with cross-gradients (cross section at y = 5000 m): (a) velocity, (b) density. The gravity color scale spans the interval $[2070, 2725]$ kg/m^3, which is the same range as the density synthetic model.

was obtained after standard MT processing, which comprises some iterations of our single-domain MT inversion. We proceeded in this way to properly resemble the way our SJI software is used in practice; the MT expert sets the initial resistivity model following his criteria, and the seismic expert sets the initial velocity model following possibly different criteria. So we have initial seismic and resistivity models that are obtained with independent procedures. For resistivity we had $1\ \Omega \cdot m$ for the sediments and $8\ \Omega \cdot m$ for the salt. Contrary to the workflow used to process the seismic volume, we did not restrict the inversion region for MT. Again, this choice resembles what often happens in practice: usually SJI is performed after a starting model of reasonable quality has been obtained for both the resistivity and the velocity domains. These models are the result of disjoint MT and seismic inversion workflows, which have a different speed of convergence. Furthermore, single-domain CIP tomography is often performed with a layer-stripping procedure, an approach that provides successive models that are fully resolved only in some portions. On the other hand, MT successive inversions are usually performed for the whole model. The present real data example is configured in the worst case where one domain needs localized updates and the other domain does not. Furthermore, it shows how our algorithm is so flexible as to allow the MT and the seismic experts to continue to think and work as usual with the model domains to which they are more accustomed, simply because it is not required at all for SJI to be performed from the beginning of the whole processing. Figure 12 shows that the final resistivity coming from single-domain MT inversion was not significantly different from that obtained with SJI.

We can see from Figure 11 that SJI refills the removed portion of the salt better than the single-domain inversion. Furthermore, the SJI result not only suggests a new interpretation of the allochthonous base of the salt, but also the interpretation of the top of the autochthonous salt, consistent with the indication of a deep high-velocity zone. This zone was not visible in the output coming from single-domain seismic inversion (Figure 11, left) and was introduced by the link with the MT domain. Seismic inversion alone could not be able to detect the autochthonous salt, simply because our data did not provide any ray coverage there. We are quite confident of the existence of the

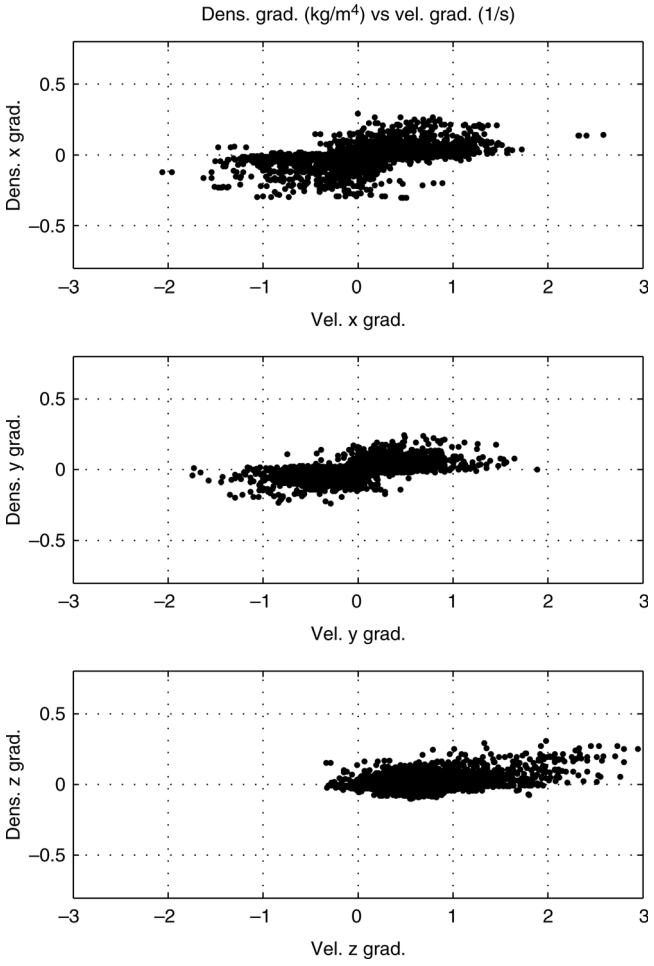

Figure 8. Crossplot velocity/density of the three gradient components of the output models resulting from separate single-domain inversions on synthetic data. Both inversions tried to invert the same shapes, but without an imposed link constraint between the two domains. This produces a weak correlation between gradients.

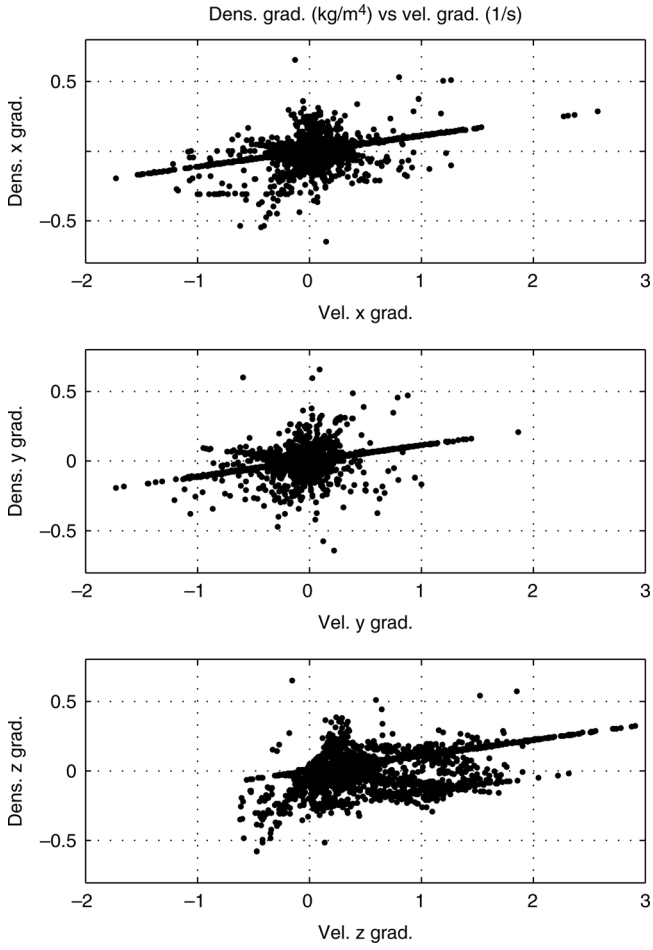

Figure 9. Crossplot velocity/density of the three gradient components of the output models resulting from a joint inversion on synthetic data with the cross-gradients constraint. The points are primarily located along a straight line with the same slope in all three plots caused by the parallelism of the main gradients.

autochthonous salt, because our 1D MT inversions also detect a deep high-resistivity zone below the allochthonous salt. As shown in Figure 13, the 1D MT inversion detects the allochthonous salt until about 6000 m of depth. Starting at about 13000 m, we see that the resistivity is rising again (and this is the beginning of the autochthonous salt). For this reason, we know that the deep high-resistivity zone, which is transferred into a high-velocity zone by SJI, is not an inversion artifact. Furthermore, seismic inversion alone could not detect this zone because we did not invert any depth moveout residuals there.[4] Finally, remigration with a new model built on the basis of the new interpretations produced with SJI results gives a better quality subsalt image (Figure 14).

DISCUSSION

We think that the method we proposed for the implementation of SJI gave good results both on synthetic and real datasets; however, this is not the only way. We found a very interesting approach to SJI presented by Haber and Oldenburg (1997). Their approach is to minimize a measure of the difference in structure between two models, given by

$$\phi_c = \int (S[m_1] - S[m_2])^2 dV \tag{18}$$

subject to

$$\phi_d = \left\| F^{(1)}[m_1] - d_1 \right\|^2 + \left\| F^{(2)}[m_2] - d_2 \right\|^2 = \phi_d^* \tag{19}$$

where ϕ_d^* is a target misfit and

$$S[m] = \begin{cases} 0 & \left|\nabla^2 m\right| < \tau_1 \\ P_5\left(\left|\nabla^2 m\right|\right) & \tau_1 < \left|\nabla^2 m\right| < \tau_2 \\ 1 & \tau_2 < \left|\nabla^2 m\right| \end{cases} \tag{20}$$

and τ_1 and τ_2 must be chosen by the user; P_5 is a polynomial in one dimension with degree five that makes the structure operator twice Frechet differentiable. The application of this structural link is promising because it is scaled by definition between zero and one. The drawback is that the results depend on the choice of τ_i parameters, and a robust method to choose them must be devised. Anyway this could be a useful addition to our set of links.

Gallardo and Meju (2004) use a similar approach, but the minimization is done on the sum of single-domain objective functions, subject to the cross-gradients constraint.

We reckon that these techniques are all valid ways to solve the SJI problem, but we also think that using single-domain objective

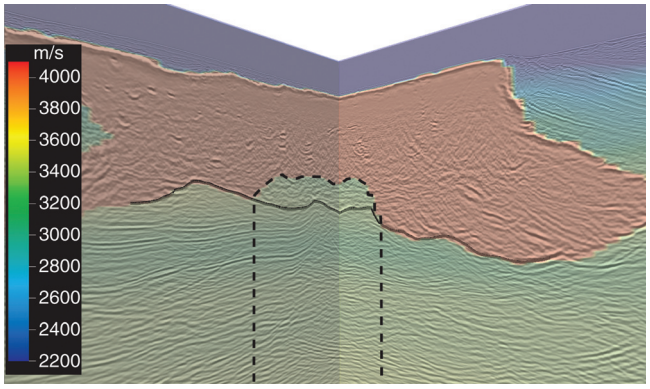

Figure 10. Initial model used for inverting Walker Ridge data. A portion of salt has been removed from the bottom (black, continuous line). The salt has a velocity of about 4500 m/s. In this figure, the modification has already been applied. The modified zone is the one located between the continuous and the dashed lines. The dashed line denotes the zone that will be inverted by the seismic CIP tomography.

[4]Depth moveouts are the data in a CIP tomography inversion.

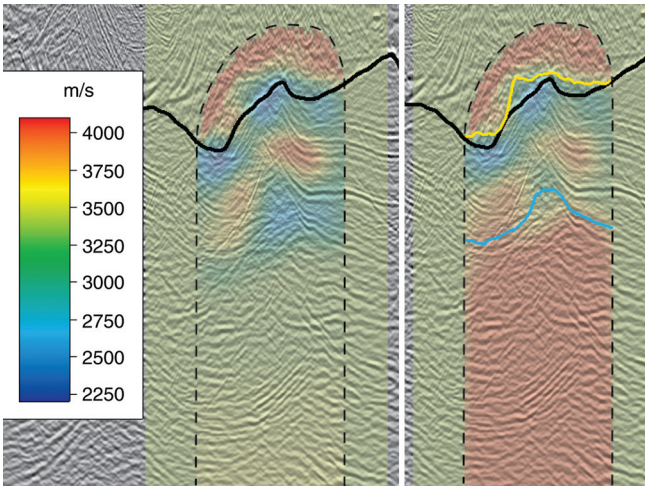

Figure 11. CIP tomography output. Left: single-domain inversion. Right: SJI with interpretations. Dashed line: inversion zone. Continuous black line: bottom of the salt before the inversion. Yellow line: new interpretation of the salt bottom. Cyan line: interpretation of the autochthonous top salt.

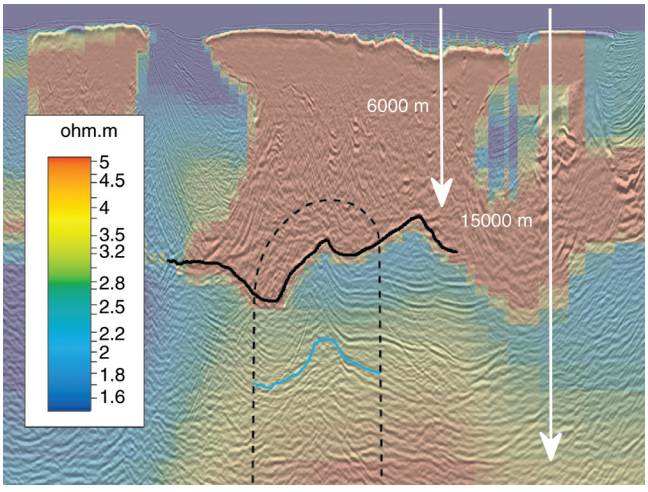

Figure 12. Final MT model from SJI. Black line is the salt bottom. Dashed line is the inversion zone for the CIP tomography. Cyan line is the interpretation of the autochthonous top salt (the same as the one in Figure 11). Inversion in the MT domain modifies the whole model, not only a portion, like CIP tomography.

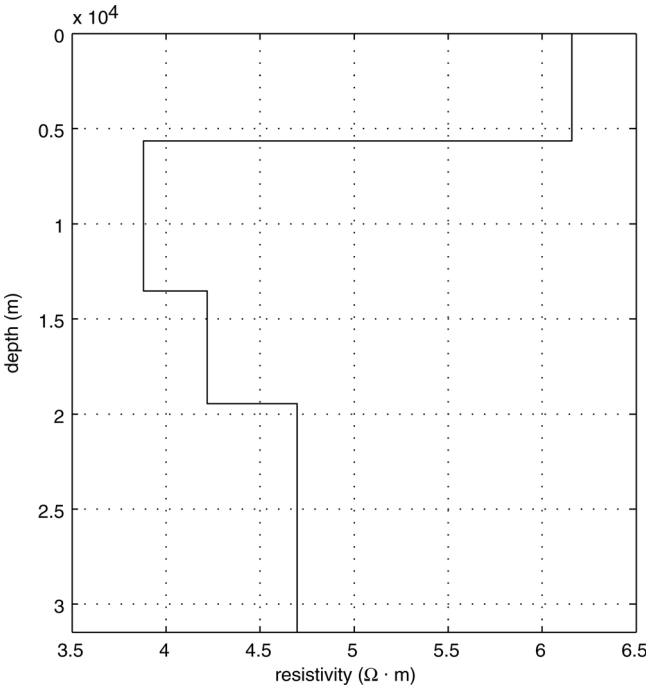

Figure 13. 1D MT inversion of data recorded by a station above the middle of the model of Figure 12. This curve confirms the existence of an autochthonous salt (resistivity rises again starting from about 13000 m) below the allochthonous one (resistivity decreases at about 6000 m).

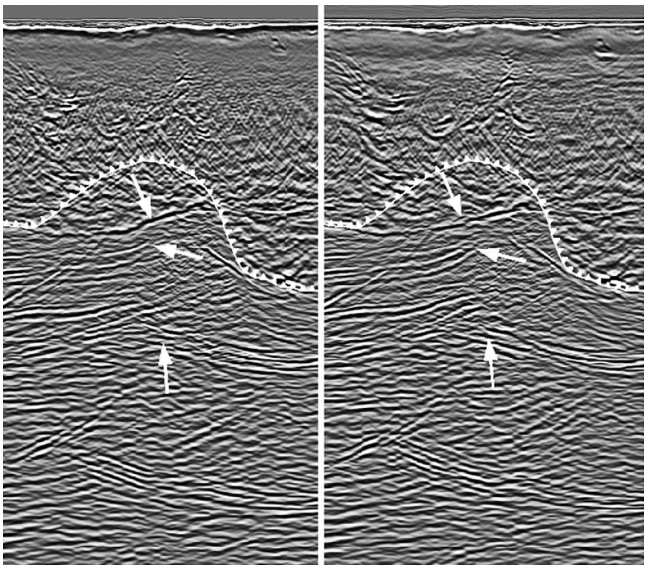

Figure 14. Subsalt detail of the PSDM sections using a single-domain velocity model (left) and an SJI velocity model (right). The line with triangular markers runs on the salt bottom with the hole created by us. The regions with the main improvements are indicated by the white arrows.

functions and linking objective functions without differentiating between "function to be minimized" and "constraint" (like we do with equation 1) allows us to apply the formulation also in cases where the link is not strictly exact for the geological region of interest, with a resulting wider applicability. In fact, this is the key difference that allowed us to include this algorithm into real production workflows.

Another interesting paper that shows some successful results of SJI application is that by Jegen et al. (2009). Their approach requires a starting seismic model, converting it through empirical, possibly space-variant, laws into starting density and resistivity models, and performing an SJI between these two. The result is a gravity-MT SJI with the cooperation of a seismic a priori model. Even if that paper does not present a formulation of the objective function that gets optimized, it shows a link between velocity and density that is basically the same as that proposed in equation 7. The link between velocity and resistivity is essentially the same but in logarithmic form. In fact, taking the logarithm on both sides of equation 7 drives us to the formulation presented by Jegen et al. (2009). This confirms that the parametric Gardner's law of equation 7 can be effectively used in a variety of situations.

Although it is effective, our algorithm can still be improved on several aspects. First of all, some further research has to be done to allow an automatic calibration of the weights of the different components of equation 1. Some help could be found by exploring the theory of automatic controls or trying to adapt the techniques for choosing hyperparameters to SJI (see Ulrych et al., 2001; Malinverno and Briggs, 2004). We still think that the user should have the possibility to change those weights; however, an automatically computed default value would be of invaluable help. Other possible improvements could be achieved trying inversion algorithms different from the NLCG. For example, the Broyden-Fletcher-Goldfarb-Shanno (BFGS) method (see Broyden, 1970; Fletcher, 1970; Goldfarb, 1970; Shanno, 1970; Shanno and Kettler, 1970) seems promising for achieving faster convergence (even if it requires more memory).

Another great improvement could be achieved if the SJI problem is reformulated removing the Gaussianity assumption to solve it with Monte-Carlo methods. By adapting the techniques explained by Mosegaard and Tarantola (1995), Ulrych et al. (2001) and Malinverno and Briggs (2004), practical ways for implementation could be found. We are quite confident that these approaches could bring a more complete understanding of the posterior probability density and, as a consequence, a more precise characterization of the uncertainties of the solution.

CONCLUSIONS

We have described an effective implementation of the SJI technique that minimizes a combination of linked single objective functions. The algorithm is general and does not impose a limit to the number of domains or links or require that the different domains be sampled in the same way. Therefore, new single-domain inversions can always be integrated with those already present that is allowed by our object-oriented generic implementation.

We have proposed two kinds of links: geometrical and empirical. For geometrical links, we presented the cross-gradients constraint. For empirical links, we proposed use of Gardner's law and a log-linear law. Although we used Gardner's law to link density to velocity and the log-linear law to relate

resistivity to velocity, these equations are parametric and can potentially be adapted to several situations. We have shown that these two types of links are effective on synthetic and real data sets.

Application of our methods to synthetic data sets demonstrated the benefits of using SJI with respect to separate, single-domain inversions. Analysis of synthetic results showed that geometrical links are primarily useful when no empirical link is known between the domains that we want to jointly invert. Empirical links are preferable even if they can be extrapolated from other geological information such as well logs.

Simultaneous joint inversion of field data confirmed the effectiveness of the technique. If properly tuned, SJI may obtain final models that simultaneously integrate features visible only in some (or even only one) of the involved domains. Furthermore, the results obtained with real data on the Walker Ridge area in the Gulf of Mexico allowed us to improve the quality of the subsalt image. Most importantly, SJI defines a new strategy for subsalt interpretation, thereby enhancing the role of nonseismic methods to support complex seismic depth imaging. SJI is a more constrained inversion with respect to single-domain inversions, simply because the single components are inverted together. For this reason, the intrinsic nonuniqueness of the electromagnetic and gravity inverse problems was reduced, improving the resolution, accuracy, and value of nonseismic data domains.

ACKNOWLEDGMENTS

The work on the parallel, 3D SJI started in January 2007, supported first by Geosystem S.r.l. and then by WesternGeco. There were many people that, directly or indirectly, contributed to the success of this technique.

Several colleagues helped us. Randall Mackie is thanked for supporting the MT inversion algorithm. Marta Woodward, Michael O'Briain, and Stephen Alwon (DP and R&D in Houston) are thanked for their support in generating the workflow and the seismic information for SJI. Don Watts and Stephen Hallinan (Milan) provided the know-how and applications for nonseismic applications. The Geo-Exploration team in Houston provided the interpretations, the geological background, and most importantly, the strategic vision for SJI in Gulf of Mexico applications. Dave Nichols (Houston) is thanked for providing the NLCG solver.

We thank all PETSc developers, particularly Matthew Knepley (University of Chicago), Barry Smith, Hong Zhang, and Satish Balay (Argonne National Laboratories, Mathematics and Computer Science Division, Chicago) for their support. Thanks also to Lisandro Dalcin at Centro Internacional de Métodos Computacionales en Ingeniería (CIMEC), Santa Fe, Argentina, for his support to the petsc4py Python package.

REFERENCES

Andersen, H. T., and T. R. Bodger, July, 2005, Integration of seismic and non-seismic methods for hydrocarbon exploration; a Bolivian case history: Geohorizons, 27–29.

Balay, S., K.Buschelman, V.Eijkhout, W. D.Gropp, D. Kaushik, M. G. Knepley, L. C. McInnes, B. F. Smith, and H. Zhang, 2008, PETSc users manual: Technical Report ANL-95/11-Revision 3.0.0, Argonne National Laboratory.

Balay, S., K. Buschelman, W. D. Gropp, D. Kaushik, M. G. Knepley, L. C. McInnes, B. F. Smith, and H. Zhang, 2009, PETSc Web page. (http://www.mcs.anl.gov/petsc).

Balay, S., W. D. Gropp, L. C. McInnes, and B. F. Smith, 1997, Efficient management of parallelism in object oriented numerical software libraries: Modern Software Tools in Scientific Computing, Birkhäuser Press, 163–202.

Berdichevsky, M. N., and V. I. Dmitriev, 2002, Magnetotellurics in the context of the theory of ill-posed problems: Society of Exploration Geophysicists, Investigations in Geophysics, **11**.

Broyden, C. G., 1970, The convergence of a class of double-rank minimization algorithms: IMA Journal of Applied Mathematics, **6**, no.1, 76–90, doi:10.1093/imamat/6.1.76.

Campbell, T. F. Snyder, X. Wu, S. Sandberg, and C. Campbell, 2009, Subsalt seismic image enhancement using multi-measurements in the Gulf of Mexico: Presented at the PETEX 2009 edition, PESGB.

De Stefano, M., and D. Colombo, 2007, Pre-stack depth imaging via simultaneous joint inversion of seismic, gravity and magnetotelluric data: Presented at the 69th EAGE Conference and Exhibition, EAGE, Extended Abstracts.

Dell'Aversana, P., Integration of seismic, Mt and gravity data in a thrust belt interpretation: First Break, **19**, 335–341 (2001).

Fletcher, R., 1970, A new approach to variable metric algorithms: The Computer Journal, **13**, no.3, 317–322, doi:10.1093/comjnl/13.3.317.

Fu, L. Y., 2004, Joint inversion of seismic data for acoustic impedance: Geophysics, **69**, no.4, 994–1004, doi:10.1190/1.1778242.

Gallardo, L. A., and M. A. Meju, 2004, Joint two-dimensional dc resistivity and seismic travel time inversion with cross-gradients constraints: Journal of Geophysical Research, **109**, B3, B03311, doi:10.1029/2003JB002716.

Goldfarb, D., 1970, A family of variable-metric methods derived by variational means: Mathematics of Computation, **24**, no.109, 23–26, doi:10.1090/S0025-5718-1970-0258249-6.

Haber, E., and D. Oldenburg, 1997, Joint inversion: a structural approach: Inverse Problems, **13**, no.1, 63–77, doi:10.1088/0266-5611/13/1/006.

Hu, W., A. Abubakar, and T. M. Habashy, 2009, Joint electromagnetic and seismic inversion using structural constraints: Geophysics, **74**, no.6, R99–R109, doi:10.1190/1.3246586.

Jegen, M. D., R. W. Hobbs, P. Tarits, and A. Chave, 2009, Joint inversion of marine magnetotelluric and gravity data incorporating seismic constraints. Preliminary results of sub-basalt imaging off the Faroe Shelf: Earth and Planetary Science Letters, **282**, no. 1-4, 47–55, doi:10.1016/j.epsl. 2009.02.018.

Li, Y., and D. W. Oldenburg, 1996, 3-D inversion of magnetic data: Geophysics, **61**, no.2, 394–408, doi:10.1190/1.1443968.

Li, Y., and D. W. Oldenburg, 1998, 3-D inversion of gravity data: Geophysics, **63**, no.1, 109–119, doi:10.1190/1.1444302.

Li, Y., and D. W. Oldenburg, 2000, Joint inversion of surface and three-component borehole magnetic data: Geophysics, **65**, no.2, 540–552, doi:10.1190/1.1444749.

Mackie, R., Rodi W., and M. Watts, 2001, 3D magnetotelluric inversion for resource exploration: 71st Annual International Meeting, SEG, Expanded Abstracts, 1501–1504.

Mackie, R., L., and T. R. Madden, 1993, Conjugate direction relaxation solutions for 3-D magnetotelluric modeling: Geophysics, **58**, no.7, 1052–1057, doi:10.1190/1.1443481.

Mackie, R. L., T. R. Madden, and P. E. Wannamaker, 1993, Three-dimensional magnetotelluric modeling using difference equations—Theory and comparisons to integral equation solutions: Geophysics, **58**, no.2, 215–226, doi:10.1190/1.1443407.

Malinverno, A., and V. Briggs, 2004, Expanded uncertainty quantification in inverse problems: Hierarchical Bayes and empirical Bayes: Geophysics, **69**, no.4, 1005–1016, doi:10.1190/1.1778243.

Mosegaard, K., and A. Tarantola, 1995, Monte carlo sampling of solutions to inverse problems: Journal of Geophysical Research, **100**, B7, 12 431–12447, doi:10.1029/94JB03097.

Osypov, K., D. Nichols, M. Woodward, and C. E. Yarman, 2008, Tomographic velocity model building using iterative eigen decomposition: Presented at the 70th EAGE Conference and Exhibition, EAGE, Extended Abstracts.

Pratt, W. K., 1991, Digital image processing, 2 ed.: John Wiley & Sons.

Rossi, G., and A. Vesnaver, 1997, 3-D imaging by adaptive joint inversion of reflected and refracted arrivals: 67th Annual International Meeting, SEG, Expanded Abstracts, 1873–1876.

Shanno, D. F., 1970, Conditioning of quasi-Newton methods for function minimization: Mathematics of Computation, **24**, no.111, 647–656, doi:10.1090/S0025-5718-1970-0274029-X.

Shanno, D. F., and P. C. Kettler, 1970, Optimal conditioning of quasi-Newton methods: Mathematics of Computation, **24**, no.111, 657–664, doi:10.1090/S0025-5718-1970-0274030-6.

Tarantola, A., 2005, Inverse Problem Theory and methods for model parameter estimation: SIAM.
Teukolsky, S. A., W. T. Vetterling, and B. P. Flannery, 2007, Numerical recipes—the art of scientific computing: William H. Press.
Ulrych, T. J., M. D. Sacchi, and A. Woodbury, 2001, A Bayes tour of inversion: A tutorial: Geophysics, **66**, no.1, 55–69, doi:10.1190/1.1444923.
Woodward, M. J., P. Farmer, D. Nichols, and S. Charles, 1998, Automated 3-D tomographic velocity analysis of residual moveout in prestack depth migrated common image point gathers: 68th Annual International Meeting, SEG, Expanded Abstracts, 1218–1221.
Yang, C. H., and L. T. Tong, 1988, Joint inversion of DC, TEM, and MT data: 58th Annual International Meeting, SEG, Expanded Abstracts, Session: POS1.2.
Zhang, J., R. L. Mackie, and T. R. Madden, 1995, 3-D resistivity forward modeling and inversion using conjugate gradients: Geophysics, **60**, no.5, 1313–1325, doi:10.1190/1.1443868.